nature chemistry

ARTICLES

https://doi.org/10.1038/s41557-018-0060-5

Identification and characterization of diverse coherences in the Fenna–Matthews–Olson complex

Erling Thyrhaug[1,5], Roel Tempelaar[2], Marcelo J. P. Alcocer[1], Karel Žídek[1,6], David Bína[3], Jasper Knoester[4], Thomas L. C. Jansen[4] and Donatas Zigmantas[1*]

The idea that excitonic (electronic) coherences are of fundamental importance to natural photosynthesis gained popularity when slowly dephasing quantum beats (QBs) were observed in the two-dimensional electronic spectra of the Fenna–Matthews–Olson (FMO) complex at 77 K. These were assigned to superpositions of excitonic states, a controversial interpretation, as the strong chromophore–environment interactions in the complex suggest fast dephasing. Although it has been pointed out that vibrational motion produces similar spectral signatures, a concrete assignment of these oscillatory signals to distinct physical processes is still lacking. Here we revisit the coherence dynamics of the FMO complex using polarization-controlled two-dimensional electronic spectroscopy, supported by theoretical modelling. We show that the long-lived QBs are exclusively vibrational in origin, whereas the dephasing of the electronic coherences is completed within 240 fs even at 77 K. We further find that specific vibrational coherences are produced via vibronically coupled excited states. The presence of such states suggests that vibronic coupling is relevant for photosynthetic energy transfer.

Through billions of years of evolution, nature has found a solution for the efficient harvesting of sunlight in the form of densely packed pigments embedded in protein environments[1,2]. In aiming to understand the functionality of these complexes, particular attention has been paid to the Fenna–Matthews–Olson (FMO) complex[3], a small protein homo-trimer situated between the chlorosome antennae and the photosynthetic reaction centre (RC) of green sulfur bacteria.[4,5] This historic interest in the FMO complex has been due to the early resolution of its crystal structure[6,7], its relative structural simplicity (Fig. 1a) and its high water solubility. Together, these properties make the complex both experimentally accessible and simple enough to allow for detailed theoretical work. The assumption has thus been that it could serve as an exemplar system to unravel the mechanisms that underlie photosynthetic light harvesting. Decades of experimental and theoretical studies have thus resulted in detailed descriptions of the excitonic structure and energy-transfer dynamics[8–13], and recent two-dimensional electronic spectroscopy (2DES)[14,15] studies have enabled direct tracking of the energy flow in both isolated[9,16] and in situ[5] complexes.

The prevailing model for energy transfer in weakly or intermediately coupled systems such as the FMO complex is based on incoherent excitation 'hopping'[17], with models based on this picture being highly successful in explaining energy transfer in a wide variety of photosynthetic complexes. In 2007, a strongly contrasting picture received significant attention when long-lived quantum beats (QBs) were reported in the 2DES signals of the FMO complex at 77 K (refs [18,19]) and attributed to coherent superpositions of excitonic states. Excitonic coherence had already been identified in 1997[20], but the dephasing time was then estimated to be less than ~180 fs even at 19 K. Although this suggested a very limited timespan of excitonic superpositions, in particular at physiological temperatures, subsequent observations of similar QBs in the 2DES signals from other photosynthetic complexes were interpreted to imply that such coherence dynamics could be crucial to photosynthetic function[21–23].

Since its proposition, this coherent excitonic interpretation has been highly controversial, as the broad homogeneous spectral lines of light-harvesting complexes[24] suggest strong coupling of electronic states to the environment and, as a consequence, fast dephasing. To overcome this apparent contradiction, correlated site energy fluctuations for the protein-bound pigments were proposed[18,25]. Subsequent simulations failed, however, to identify any such 'protection' of coherences[26,27].

Recently, a mutagenesis approach made it possible to investigate the dynamics of FMO complexes with substantially different energy-level structure[28]. Contrary to expectation, given by an excitonic coherence interpretation, the observed long-lived QBs appeared to have a negligible dependence on the exciton energies. Moreover, theoretical studies indicated that the observed spectroscopic signals could be explained by vibronic coupling of excited states. Several excitonic energy gaps in the FMO complex are found at around 150–240 cm^{-1}, a range that contains a number of weakly Franck–Condon active ring-deforming vibrational modes of the bacteriochlorophyll a (BChl) molecules[29–31]. By explicitly incorporating such modes into a vibronic exciton model, it was shown that long-lived coherences of a mixed vibronic character could be produced in the excited state[32]. Later it was demonstrated that ground-state vibrations also can produce signals similar to those observed in the FMO complex[33] when excited via vibronically coupled transitions. A subsequent study that incorporated the entire FMO subunit concluded that ground-state coherences, in fact, dominate the 2DES signal.[34]

In this study we apply extensive analysis of the QBs in data obtained from two distinct sequences of polarized pulses to

[1]Chemical Physics, Lund University, Lund, Sweden. [2]Department of Chemistry, Columbia University, New York, NY, USA. [3]Biology Centre CAS and Faculty of Science, University of South Bohemia, České Budějovice, Czech Republic. [4]University of Groningen, Zernike Institute for Advanced Materials, Groningen, the Netherlands. Present address: [5]Fakultät für Chemie, Technische Universität München, Garching, Germany. [6]TOPTEC, Institute of Plasma Physics, Academy of Sciences of the Czech Republic, Prague, Czech Republic. These authors contributed equally: Erling Thyrhaug, Roel Tempelaar
*e-mail: donatas.zigmantas@chemphys.lu.se

© 2018 Macmillan Publishers Limited, part of Springer Nature. All rights reserved.

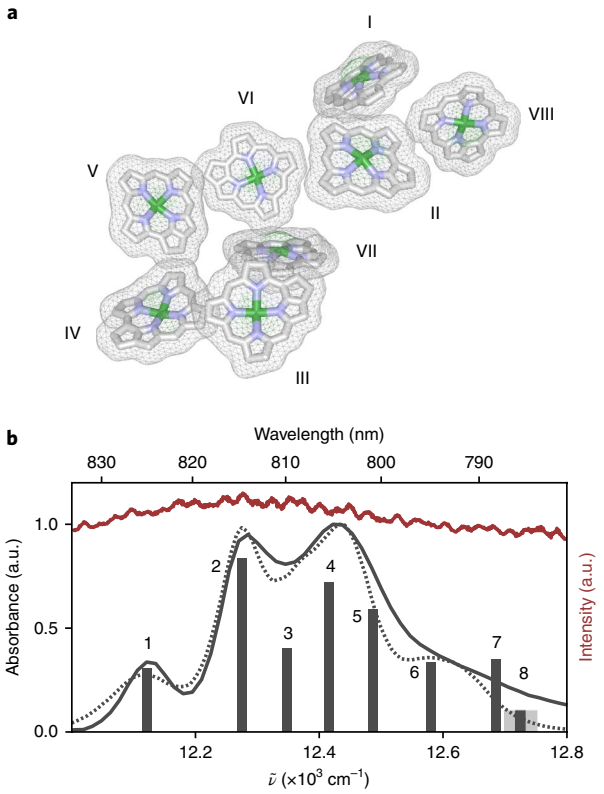

Fig. 1 | Structure and absorption of the FMO complex . a, Structural arrangement of the bacteriochlorophyll *a* molecules in the FMO complex (from published data[6]) with site numbering according to Fenna. **b**, Experimental (solid line) and calculated (broken line) absorption spectra of the FMO complex at 77 K. Experimentally determined[16] exciton energies (vertical bars) and laser spectrum (red) used in 2DES experiments are also shown. The eighth excitonic state (in the shaded area) was not included in the modelling. a.u., arbitrary units.

characterize coherences in the FMO complex at 77 K. We clearly distinguish short-lived excitonic coherences and long-lived vibrational coherences both in the ground and excited states.

Results

Structure and absorption of the FMO complex. The initial crystallographic work on the FMO complex found the protein subunits to contain well-defined structures of seven[3] (later amended to eight[6]) BChl pigments (Fig. 1a). We identified the spectroscopic signatures of the eighth BChl in a preceding FMO study[16], and we presume that the isolated FMO complexes investigated here also contain eight BChl molecules. The previously extracted exciton energies and 77 K absorption spectrum of the FMO complex isolated from the green sulfur bacteria *Chlorobium tepidum* are shown in Fig. 1b.

Coherence signals in polarization-controlled 2DES. The 2DES technique[15] and our specific implementation[35] have been detailed previously. The recorded data set appears as a sequence of two-dimensional (2D) maps in which the complex emitted field, $E^{(3)}(\tilde{\nu}_1,t_2,\tilde{\nu}_3)$, is displayed as a function of excitation and detection energies (proportional to the wavenumbers $\tilde{\nu}_1$ and $\tilde{\nu}_3$, respectively) and evolves with the population time t_2. QBs may appear along t_2, the excitation/detection energy dependence of which can be conveniently identified by a Fourier transform over population time. We refer to the resulting maps as $\tilde{\nu}_2$ oscillation maps.

2DES data sets contain the entire third-order response of the system, and the resulting information density may lead to problematic spectral congestion in multichromophore systems. Polarization techniques can be used to alleviate such congestion, because the measured signals are dependent on both the relative angles between transition dipole moments and the relative polarization angles of the incident laser pulses. These approaches are particularly powerful in fully noncollinear 2DES geometries, where one can control the polarizations of all incident pulses and the detected signal.

Most reported studies on the FMO complex[18,19] and other photosynthetic complexes[21,23,36,37] have, nevertheless, exclusively employed a series of parallel-polarized pulses, denoted here as 'all-parallel' (AP) or ⟨0°,0°,0°,0°⟩. Although this sequence typically yields the strongest signal, it preferentially generates signals that originate from interactions between parallel dipoles. As a consequence, coherence dynamics in these experiments are dominated by intramolecular vibrational motion.

To suppress such intramolecular signals and allow the signatures of coherences across multiple pigments to emerge, we applied a sequence of two perpendicularly polarized pulse pairs, denoted here as 'double-crossed' (DC) or ⟨45°,−45°,90°,0°⟩ (Fig. 2a). First applied in 2D vibrational spectroscopy[38,39] and later in 2DES[22,40], it suppresses both all non-coherence signals (for example, population dynamics) and coherence signals that involve interactions with pairwise parallel transition dipoles. Thus, signals from localized vibrational modes are suppressed, whereas signals from, for example, intermolecular electronic coherence remain.

In coupled multichromophore systems, certain linear combinations of vibrational modes can also contribute to the DC signal[33] (the details are published elsewhere[41]). This occurs when a coherence is generated through transitions to (vibronically) mixed excited states. As detailed by Tiwari et al.[33], this results in the electronic character of the excited states taking on a vibrational coordinate dependence, which effectively causes the transition polarization to oscillate with the vibrational frequency. Vibronically coupled states are thus revealed through the presence of vibrational contributions in the DC signal.

To provide support for the experimental assignment of the coherence signals, we simulated the time evolution of the FMO subunit using a vibronic exciton model to calculate a polarization-resolved 2D spectrum at each population time step. The model (details are given in Supplementary Section 1 and published elsewhere[34]) explicitly includes a Raman-active vibrational mode for each BChl, which was parametrized with a Huang–Rhys factor of 0.02 and a wavenumber of 160 cm^{-1}. The weakly coupled eighth BChl and the weak interactions between BChls on different trimeric units were neglected, and the calculations were thus based on the seven-site electronic Hamiltonian obtained in previous studies[8]. The calculated absorption spectra of FMO are shown in Fig. 1b.

2D spectra of FMO. To characterize the coherence dynamics in the FMO complex with a high wavenumber resolution, polarization-controlled 2DES experiments were performed at 77 K, scanning the population time t_2 to 1.8 ps. The dramatic difference in the 2D spectral structure between the pulse-polarization sequences is clear from inspection of the spectra in Fig. 2b,c, in which the real (absorptive) part of representative (t_2 = 40 fs) rephasing 2D spectra are shown (the total 2D spectra are shown in Supplementary Fig. 1).

The AP spectra (Fig. 2b) are dominated by diagonal peaks associated with features in the absorption spectrum (Fig. 1b), whereas the patterns of off-diagonal features reveal correlations between the transitions. The excitonic structure and relaxation pathways that emerge from analysis of the time evolution of the 2D spectrum are detailed elsewhere[16]. In the DC spectra (Fig. 2c), signals from population dynamics are suppressed, and the remaining signals are 'running waves' across the 2D map of alternating negative and positive features. The time evolution also differs radically; whereas population dynamics dominate the AP spectra, with only weak QBs

© 2018 Macmillan Publishers Limited, part of Springer Nature. All rights reserved.

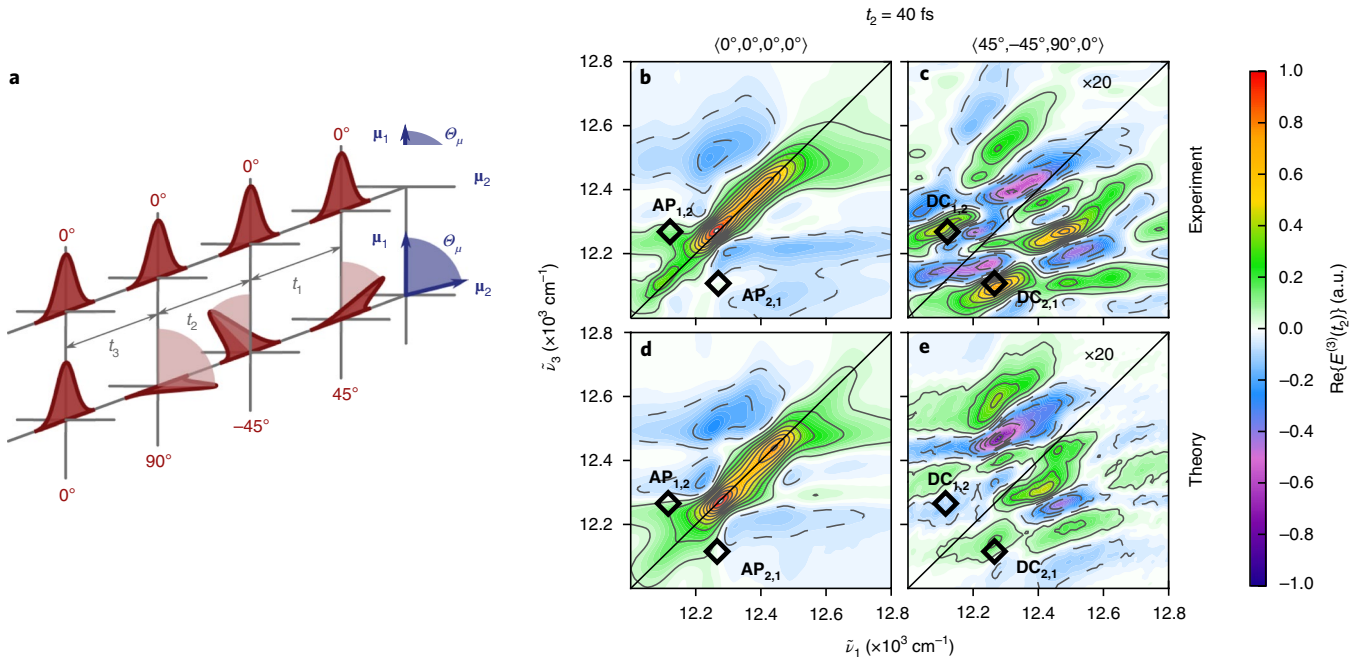

Fig. 2 | Polarization-controlled 2DES of the FMO complex . **a**, Schematic representation of the AP pulse sequence (top), which favours interaction pathways that involve parallel transition dipoles ($\boldsymbol{\mu}_1$ only), and the DC pulse sequence (bottom), which favours pathways that involve non-parallel transition dipoles ($\boldsymbol{\mu}_1$ and $\boldsymbol{\mu}_2$). The two pulse sequences were used to provide detection selectivity of the various QBs present in the 2D spectra of the FMO complex. **b**–**e**, Real part of the rephasing 2D spectra at $t_2 = 40$ fs. Experimental (**b** and **c**) and theoretical (**d** and **e**) spectra that result from AP (**b** and **d**) and DC (**c** and **e**) pulse sequences are shown. The spectra are normalized to the exciton 2 diagonal peak of the AP spectra and the DC spectra are scaled by a factor of 20 for clarity. Markers AP and DC denote the exciton 1–2 and 2–1 cross-peak positions in the appropriate spectra at which the dynamics presented in Fig. 3 are taken.

(<5% of total amplitude), the DC spectra are purely oscillatory (Supplementary Fig. 2).

Despite the great complexity in modelling the FMO spectral response, the simulated spectra (Fig. 2d,e) show good agreement with experimental data for both pulse polarization sequences. This indicates that the chosen parametrization of the model captures essential features of the complex.

FMO QBs. In both AP and DC experiments, the areas in the vicinity of the cross-peaks connecting the two lowest-energy excitons (located at $\tilde{\nu} = 12,120$ and 12,270 cm^{-1}) show particularly prominent QBs. These areas are labelled $AP_{1,2}$, $AP_{2,1}$ and $DC_{1,2}$, $DC_{2,1}$ in Fig. 2 for the AP and DC pulse sequences, respectively. We quantify the QBs by fitting the (complex) t_2 dynamics with a sum of damped complex oscillations and exponential decays:

$$E^{(3)}(t_2) = \sum_m A_m^{\mathrm{QB}} \mathrm{e}^{-(t_2/\tau_m^{\mathrm{QB}}) - i(\omega_m t + \varphi_m)} + \sum_n \left(A_n^{\mathrm{Re}} \mathrm{e}^{-t_2/\tau_n^{\mathrm{Re}}} + iA_n^{\mathrm{Im}} \mathrm{e}^{-t_2/\tau_n^{\mathrm{Im}}}\right) \quad (1)$$

where A are the amplitudes, ω (positive or negative) the angular frequencies, φ the phases, τ the decay time constants and $m, n = 1, 2, 3$. m indexes three oscillating components and n exponential decays. The experimental t_2 dynamics after subtraction of the population dynamics are presented in Fig. 3a, where the data are overlaid with the oscillatory components of the fits. Full fits and parameters are presented in Supplementary Section 4.

The initial cross-peak dynamics are dominated by a high-amplitude QB component, which decays completely within 240 fs. Although an accurate frequency cannot be extracted due to the subcycle dephasing times, the approximate oscillatory periods are consistent with the energy splitting between the two lowest-energy excitons. The dephasing time of 50–150 fs (Supplementary Table 1), is further consistent with the decay of excitonic coherence observed in previous cryogenic pump–probe experiments[20]. We thus attribute the rapidly dephasing QBs to coherent superpositions of excitonic states. Comparison of our results with those of Savikhin et al.[20] suggests that the signals at 77 K are dominated by intrinsic dephasing rather than by ensemble-induced dephasing (Supplementary Section 5). It is noteworthy that in a recent 2DES study[42] no substantial low-frequency coherences were observed in the FMO complex at ambient temperature, interpreted to suggest an excitonic coherence dephasing timescale of 60 fs.

The current investigation is, however, primarily concerned with the interpretation of long-lived coherences. As such, we henceforth only consider the later-time dynamics ($t_2 > 240$ fs), in which a number of QBs persist for picoseconds. To elucidate the origin of these QBs, it is instructive to consider them in the frequency (or wavenumber $\tilde{\nu}_2$) domain. The Fourier transform amplitudes of the measured and theoretical dynamics are presented in Fig. 3b, in which well-defined peaks appear at positive or negative wavenumbers. This discrimination originates from the separation of signals that evolve with opposite phase, that is, as either $\mathrm{e}^{-i\omega t_2}$ or $\mathrm{e}^{+i\omega t_2}$. This separation proves highly useful when assigning oscillatory signals to specific physical processes[43–46].

In the below-diagonal cross-peak area investigated in previous work[18,19] (labelled here as $AP_{2,1}$ and $DC_{2,1}$), the dynamics are dominated by −170 and −210 cm^{-1} modes that exhibit dephasing times of ~2 ps. This corresponds to the energies close to several excitonic gaps (Fig. 1b), and also similar wavenumber vibrational modes appear in the fluorescence line-narrowing spectra of the FMO complex[29]. Notably, we do not observe any significant higher-wavenumber features, in agreement with Fransted et al.[47] but in contrast with the initial study[18], in which coherences were reported at ~350 and ~500 cm^{-1}.

© 2018 Macmillan Publishers Limited, part of Springer Nature. All rights reserved.

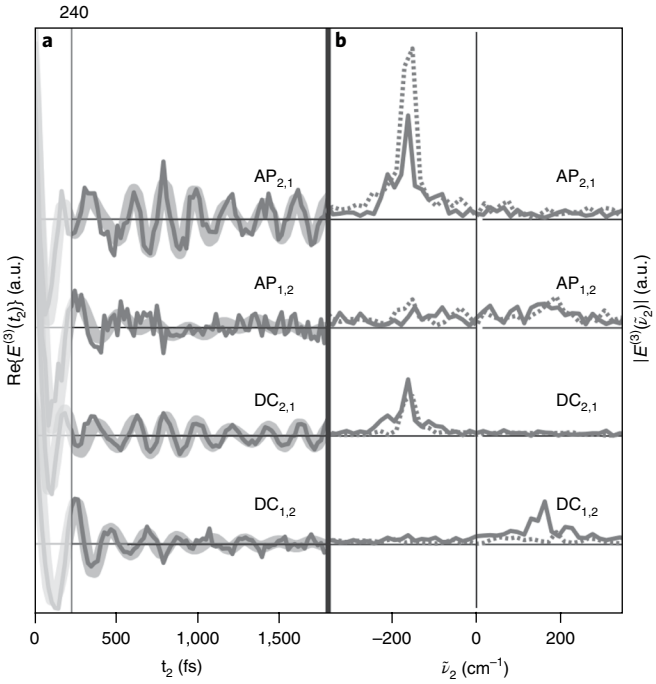

Fig. 3 | Selected QBs in FMO. a, Measured real-part rephasing t_2 traces (thin lines) at the cross-peak locations labelled in Fig. 2 after subtraction of multiexponential dynamics. Long-lived (picoseconds) QBs are clearly visible in the dynamics. Individual time-domain fits (thick lines), which correspond to the oscillatory terms in equation (1) are overlaid onto each trace (the fit parameters are given in Supplementary Table 1). The traces are not normalized, but are vertically offset for clarity. **b**, Fourier transform amplitudes of the experimental data ($t_2 > 240$ fs) shown in **a** and the theoretical vibronic exciton model data extracted from the same points (broken lines).

The behaviour of QBs at $AP_{2,1}$ and $DC_{2,1}$ and their relative amplitudes are well reproduced by the theoretical model, whose frequency domain response is also presented in Fig. 3b. In particular, the simulations clearly capture the intensity suppression imposed by the DC sequence. Note that for each BChl only the 160 cm^{-1} mode was included in the model.

The above-diagonal cross-peak, $DC_{1,2}$, however, is dominated by positive-wavenumber QBs. Although the wavenumbers extracted from time domain fits are identical to those seen below the diagonal, the dephasing times are noticeably shorter, with an average dephasing time of ~570 fs (Fig. 3 and Supplementary Table 1). These QBs are not reproduced accurately in the simulation, which suggests they arise from a mechanism not captured explicitly by the vibronic model in its current form. We discuss the origin of these QBs in the following sections.

Oscillation maps. Although useful information about the system can be inferred from single-point kinetic traces, coherence signals from multichromophore systems are complex, which leaves such an approach insufficient for unambiguous characterization. Fortunately, the complex-valued 2DES data sets contain the signatures of all Liouville (interaction) pathways supported by the laser spectrum[48]. As such, a Fourier transform of beating signals along the population time t_2 yields $\tilde{\nu}_2$ oscillation maps, which show the QB Fourier amplitude dependence on excitation- and detection-energy coordinates[43,44]. QBs of different origins produce distinct patterns and can therefore be used to unambiguously determine the origin of coherences[45].

We constructed oscillation maps from both the experimental and simulated data sets, and in Fig. 4 present the AP and DC maps at the dominant $\pm 170\ cm^{-1}$ wavenumbers. The similar, but weaker, experimental oscillation maps at $\pm 210\ cm^{-1}$ are shown in Supplementary Fig. 4.

The negative-wavenumber experimental AP map (Fig. 4a) is richest in structure, particularly in the area around $AP_{2,1}$ in which long-lived QBs were reported in previous studies[18,19]. Although the dephasing times found at $AP_{2,1}$ are in agreement with Panitchayangkoon et al.[19] (Fig. 3 and Supplementary Table 1), it is apparent that the observed $-170\ cm^{-1}$ QB is not an isolated feature, but rather forms part of a square pattern of below-diagonal peaks. Following the analysis of Butkus et al.[49], this is the characteristic signal of ground-state vibrational wavepackets.

In contrast to this, the AP positive-wavenumber map (Fig. 4b) is almost featureless, and exhibits only poorly defined areas of QB amplitude in much of the diagonal and above-diagonal regions. It is thus clear that the AP experimental results are dominated by negative-wavenumber QBs (Fig. 3b).

The experimental DC oscillation maps (Fig. 4c,d) are relatively sparse, with positive- and negative-wavenumber maps of comparable amplitude. A relatively high-amplitude peak is observed at $DC_{2,1}$ in the negative-wavenumber DC map, whereas at positive wavenumbers a significant amplitude only appears around $DC_{1,2}$. It has been pointed out elsewhere[45,46] that above-diagonal positive-wavenumber QBs in rephasing spectra, as observed in Fig. 4d, are characteristic of excited-state coherence. That this feature does not contribute significantly in the AP experiment (Fig. 4b) may be due to interference with an overlapping excited-state absorption in the same spectral region.

The simulated negative-wavenumber oscillation maps show reasonable agreement with the experiment, and the major features in both the AP and DC experiments are well captured, as seen in Fig. 4a,c,e,g. The main discrepancy is the presence of non-negligible features at higher detection wavenumbers in the simulated data. Two factors probably contribute to this: (1) the model does not reproduce perfectly the relative exciton oscillator strength, which results in an apparent signal increase for coherences that involve higher energy transitions, and (2) vibrations on all sites are assumed to have the same Huang–Rhys factor in the model, which results in additional below-diagonal square-peak arrangement, appearing at higher wavenumbers. This assumption is unlikely to be valid, as vibrations that involve exciton 2 dominate the experimental coherence response, whereas vibrations from higher-energy excitons contribute only weakly. We speculate that Herzberg–Teller coupling—a dependence of the BChl's transition dipoles on nuclear coordinates[50]—may play a role due to its influence on excited state displacements[51].

Finally, in accordance with the single-point traces (Fig. 3b), excited-state coherence appears with too small an amplitude in the simulations (Fig. 4h). This suggests that vibronic coupling effects in the excited state may not have been sufficiently accounted for and may be a fruitful area for future improvements in the modelling of the FMO complex.

Discussion and conclusions

Much of the recently published work on the FMO complex has been formulated within a framework of excitonic coherence. This interpretation has, however, been difficult to reconcile with theoretical models using realistic parameters. Here we show that all long-lived coherence signals in the FMO complex can be explained entirely within a generally well-accepted vibronic coupling framework.

Unambiguous characterization of the convoluted coherence dynamics observed in complex multichromophore systems first requires separation of the total measured signal into rephasing and non-rephasing spectra. As demonstrated above, a second effective

© 2018 Macmillan Publishers Limited, part of Springer Nature. All rights reserved.

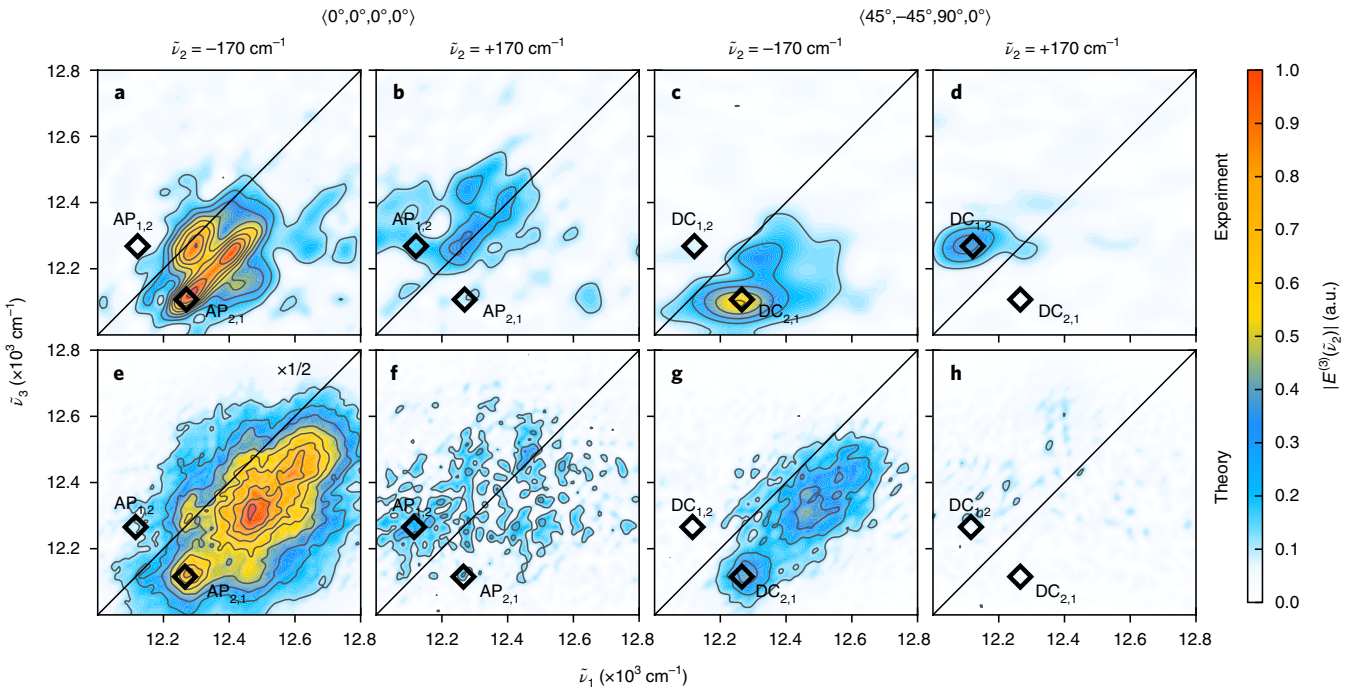

Fig. 4 | Oscillation maps. Fourier amplitude maps at ±170 cm^{-1} obtained by Fourier transformation of the 2D data sets along t_2 after subtraction of the multiexponential population dynamics. Maps for the experimental (**a**–**d**) and theoretical (**e**–**h**) data sets under the AP (**a**, **b**, **e** and **f**) and DC (**c**, **d**, **g** and **h**) pulse sequences are shown. The maps are normalized to the experimental AP$_{2,1}$ –170 cm^{-1} amplitude, and the theoretical AP –170 cm^{-1} map in **e** is scaled by a factor of 0.5 for clarity. The maps expose how QBs at this wavenumber contribute across the 2D spectra, with their pattern giving insights into coherence origins.

step is the separation of QBs into positive and negative wavenumbers, because—in the absence of coherence shifts[41]—rephasing/non-rephasing ground-state coherences only appear at negative/positive wavenumbers (Supplementary Fig. 5 gives the details). Excited-state coherences, however, exhibit as a general characteristic equal-amplitude contributions of both signs[45,46]. Consideration of the contributing Liouville pathways and of the signal sign thus allows identification of the characteristic spectroscopic 'fingerprints' of different coherences.

The strongest overall QB contribution (for both 170 and 210 cm^{-1} modes) is the negative-wavenumber below-diagonal square in the AP experiment. This is characteristic of ground-state vibrations[45,49], an assignment that is supported by our simulations. Conversely, it is entirely inconsistent with excited-state (excitonic or vibrational) coherence. As a consequence, we can directly exclude significant contributions from long-lived excitonic coherences in both our experiment and previous measurements of the FMO complex. Instead, we observe the signals from excitonic coherences as early-time QBs, dephasing on a ~100 fs timescale (Fig. 3a).

The AP experiment is limited in that it does not reveal much information about the nature of the excited states involved in generating a given coherence. In this regard, the DC experiment is more illuminating; the absence of QB signals here would imply the involvement of only 'trivial' localized states. As can be seen in Figs. 3 and 4, however, there are strong QB signals present in the DC experiment—a clear signature of vibronic coupling that leads to mixed excited states.

As QBs of both positive and negative wavenumbers contribute in the DC experiment, excited-state coherences necessarily contribute[45,46]. These cannot, however, originate from electronic coherences, as the timescale for dephasing of the positive-wavenumber contribution (τ^{QB} = 570 fs) is substantially longer than the timescale of electronic energy transfer (~350 fs (ref. [46])). It is, however, consistent with the predicted signal from the excited-state vibrations proposed in the vibronic exciton model by Christensson et al.[32]. Thus, our measurements provide an unambiguous experimental observation of excited-state vibronic coherence in the FMO complex.

The excited state cannot be the only contributor in the DC experiment, however, as the symmetry between the negative and positive oscillation maps is limited[49]. Although excited-state coherence does produce pairs of cross-peak features (such as at DC$_{1,2}$ and DC$_{2,1}$), these—because of the symmetry of the involved Liouville pathways—necessarily appear with equal amplitudes and dephasing times. We, however, observed a substantially higher QB amplitude and longer average dephasing time at DC$_{2,1}$. This strong negative-wavenumber feature (Fig. 4c) dephases in ~2 ps, which suggests the same physical origin as for the below-diagonal square in the AP experiment. Following the analysis of Jonas and co-workers[33], we can directly assign this contribution to ground-state vibrational coherence, enhanced via the vibronically coupled excitonic state at 12,270 cm^{-1}. Our simulations support this assignment, as the experimentally observed negative-wavenumber QB at DC$_{2,1}$, which originates mostly from the ground state, is reproduced successfully.

Although we have thus explained all the observed coherences in the FMO complex, the absence of higher-wavenumber (>210 cm^{-1}) vibrational modes prominent in fluorescence line narrowing experiments[29] is notable. It is possible that the dominance of low-frequency modes is due to Herzberg–Teller coupling[50], which acts to modulate the effective Huang–Rhys factors in coupled systems. Strong enhancement of low-wavenumber QBs has been observed in both porphyrin aggregates[52] and chlorosomes[53], for which simple modelling showed an enhancement of the Huang–Rhys factors of low-frequency modes through the Herzberg–Teller effect.

In summary, we have demonstrated that polarization-controlled 2DES, aided by theoretical modelling, allows for a clear interpretation of the rich coherence dynamics of the FMO complex. The conclusion is that the long-lived (picoseconds) QBs previously assigned to

© 2018 Macmillan Publishers Limited, part of Springer Nature. All rights reserved.

excitonic coherences are predominantly of ground-state vibrational origin—a finding in line with recent theoretical work[33,34]. Through their modulation of the transition polarization, these coherences reveal vibronic mixing in the electronic structure, whose impact on energy transfer is yet to be elucidated. Although the early times are dominated by excitonic coherences induced by the broadband laser excitation, the fast (~100 fs) dephasing at cryogenic temperatures combined with their notable absence in room-temperature 2DES experiments[42] implies negligible lifetimes under physiological conditions. Such short timescales strongly suggest that electronic coherences do not contribute to energy transfer in FMO, even under the speculative assumption that such superposition states can be prepared by energy transfer from the chlorosome under natural conditions.

We believe the demonstrated approach is generally applicable in disentangling the complex coherence signals of light-harvesting complexes, and thus provides a stimulus to ongoing research aimed at unravelling the role of vibronic coupling in energy transfer within photosynthetic systems.

Methods

***C. tepidum* culture and preparation of the FMO complex.** The FMO complex was isolated according to Wen et al.[54] from *C. tepidum* TLS (DSM 12025) grown in modified Pfennig medium[55] under continuous incandescent illumination at 45 °C. Cells were disrupted with EmulsiFlex C5 (Avestin Inc.) at 20,000 p.s.i. (1.03×10^6 torr). The FMO complex was released from the cell membrane using Na_2CO_3 (48 h, 0.4 M final concentration) and, after dialysis for 72 h against 20 mM Tris–HCl, pH 8, purified by size-exclusion and anion-exchange chromatography until A_{271}/A_{371} of the preparation fell below 0.6. All the steps were done at 4 °C. Prior to the 2DES experiments, the sample was dissolved in a 2:1 glycerol:buffer solution, and was held at 77 K in a nitrogen-flow cryostat during the entire experiment.

Experiment. The specifics of the non-collinear 2DES experimental set-up utilized are described elsewhere[16,35]. Briefly, broadband femtosecond pulses—approximately 100 nm in bandwidth and centred at 805 nm—were generated by a home-built non-collinear optical parametric amplifier seeded by the 1,030 nm output of a Yb:KGW amplified laser system (Pharos, Light Conversion). The resulting pulses were compressed to 14 fs using a combination of chirped mirrors and a prism compressor. The output pulses were split into two using a beamsplitter, and further split into two phase-locked pulse pairs using a diffractive optic. The linear polarizations of all four pulses were independently controlled using a quarter-wave plate and four linear wire-grid polarizers—one in each beam. The delay between the pulses of the phase-locked pair (t_1) was controlled using a fused silica wedge pair, whereas the delay between the pulse pairs (t_2) was controlled using an optical delay stage. t_1 was scanned in 1.8 fs steps until the signal decayed into noise (−270 to +450 fs and −130 to +230 fs for the AP and DC experiments respectively). The resulting spectral resolutions on the excitation axis were 36 and 72 cm^{-1}, respectively, whereas the resolution on the detection axis was 40 cm^{-1} in both experiments. t_2 was scanned in 20 fs steps from 0 to 1.8 ps. The signal-to-noise ratio was increased by averaging two consecutive scans for the AP data set and five scans for the DC data set. The estimated suppression of the signals that involved interactions with pairwise parallel dipoles in the DC measurement is ~125 times.

Modelling. Calculations were based on earlier electronic parametrizations of the FMO complex from *C. tepidum*[6,8,9]. The quantum-mechanical degrees of freedom were described using the Holstein Hamiltonian[56], which explicitly accounts for linear coupling of the electronic transition to a single vibrational mode for each BChl. In doing so, a vibrational wavenumber of 160 cm^{-1} was used in the calculations. The remaining modes were described using the overdamped Brownian oscillator model[48] with a fluctuation width and timescale consistent with molecular dynamics simulations[57]. The quantum dynamics was simulated through numerical integration of the Schrödinger equation[58,59], neglecting feedback of the quantum degrees of freedom onto the (classical) modes in the environment (effectively adapting an asymptotic high-temperature approximation for the quantum system). Absorption and 2D spectra were obtained through the evaluation of the 2-point and 4-point dipole correlation functions, respectively[48]. The absorption spectrum was averaged over 50,000 (uncorrelated) bath trajectories, whereas for the 2D spectra an average over 250,000 trajectories was taken (for details see Supplementary Section 1).

Data availability. The data presented in this study and computer codes used for theoretical simulations are available from the corresponding author upon request.

Received: 12 October 2017; Accepted: 4 April 2018;
Published online: 21 May 2018

References

1. Cogdell, R. J., Gall, A. & Köhler, J. The architecture and function of the light-harvesting apparatus of purple bacteria: from single molecules to in vivo membranes. *Q. Rev. Biophys.* **39**, 227–324 (2006).
2. Scholes, G. D., Fleming, G. R., Olaya-Castro, A. & van Grondelle, R. Lessons from nature about solar light harvesting. *Nat. Chem.* **3**, 763–774 (2011).
3. Fenna, R. E. & Matthews, B. W. Chlorophyll arrangement in a bacteriochlorophyll protein from *Chlorobium limicola*. *Nature* **258**, 573–577 (1975).
4. Hauska, G., Schoedl, T., Remigy, H. & Tsiotis, G. The reaction center of green sulfur bacteria. *Biochim. Biophys. Acta Bioenerg.* **1507**, 260–277 (2001).
5. Dostál, J., Pšenčík, J. & Zigmantas, D. In situ mapping of the energy flow through the entire photosynthetic apparatus. *Nat. Chem.* **8**, 705–710 (2016).
6. Tronrud, D. E., Wen, J., Gay, L. & Blankenship, R. E. The structural basis for the difference in absorbance spectra for the FMO antenna protein from various green sulfur bacteria. *Photosynth. Res.* **100**, 79–87 (2009).
7. Ben-Shem, A., Frolow, F. & Nelson, N. Evolution of photosystem I—from symmetry through pseudosymmetry to asymmetry. *FEBS Lett.* **564**, 274–280 (2004).
8. Vulto, S. I. E. et al. Exciton simulations of optical spectra of the FMO complex from the green sulfur bacterium *Chlorobium tepidum* at 6 K. *J. Phys. Chem. B* **102**, 9577–9582 (1998).
9. Brixner, T. et al. Two-dimensional spectroscopy of electronic couplings in photosynthesis. *Nature* **434**, 625–628 (2005).
10. Cho, M., Vaswani, H. M., Brixner, T., Stenger, J. & Fleming, G. R. Exciton analysis in 2D electronic spectroscopy. *J. Phys. Chem. B* **109**, 10542–10556 (2005).
11. Adolphs, J. & Renger, T. How proteins trigger excitation energy transfer in the FMO complex of green sulfur bacteria. *Biophys. J.* **91**, 2778–2797 (2006).
12. Savikhin, S. & Struve, W. S. Ultrafast energy transfer in FMO trimers from the green bacterium *Chlorobium tepidum*. *Biokhimiya* **33**, 11200–11208 (1994).
13. Savikhin, S., Buck, D. R. & Struve, W. S. Toward level-to-level energy transfers in photosynthesis: the Fenna–Matthews–Olson protein. *J. Phys. Chem. B* **102**, 5556–5565 (1998).
14. Hybl, J. D., Albrecht, A. W., Gallagher Faeder, S. M. & Jonas, D. M. Two-dimensional electronic spectroscopy. *Chem. Phys. Lett.* **297**, 307–313 (1998).
15. Jonas, D. M. Two-dimensional femtosecond spectroscopy. *Annu. Rev. Phys. Chem.* **54**, 425–463 (2003).
16. Thyrhaug, E., Žídek, K., Dostál, J., Bína, D. & Zigmantas, D. Exciton structure and energy transfer in the Fenna–Matthews–Olson complex. *J. Phys. Chem. Lett.* **7**, 1653–1660 (2016).
17. Vulto, S. I. E. et al. Excited state dynamics in FMO antenna complexes from photosynthetic green sulfur bacteria: a kinetic model. *J. Phys. Chem. B* **103**, 8153–8161 (1999).
18. Engel, G. S. et al. Evidence for wavelike energy transfer through quantum coherence in photosynthetic systems. *Nature* **446**, 782–786 (2007).
19. Panitchayangkoon, G. et al. Long-lived quantum coherence in photosynthetic complexes at physiological temperature. *Proc. Natl. Acad. Sci. USA* **107**, 12766–12770 (2010).
20. Savikhin, S., Buck, D. R. & Struve, W. S. Oscillating anisotropies in a bacteriochlorophyll protein: evidence for quantum beating between exciton levels. *Chem. Phys.* **223**, 303–312 (1997).
21. Collini, E. et al. Coherently wired light-harvesting in photosynthetic marine algae at ambient temperature. *Nature* **463**, 644–647 (2010).
22. Schlau-Cohen, G. S. et al. Elucidation of the timescales and origins of quantum electronic coherence in LHCII. *Nat. Chem.* **4**, 389–395 (2012).
23. Harel, E. & Engel, G. S. Quantum coherence spectroscopy reveals complex dynamics in bacterial light-harvesting complex 2 (LH2). *Proc. Natl. Acad. Sci. USA* **109**, 706–711 (2012).
24. Wendling, M. et al. Electron-vibrational coupling in the Fenna–Matthews–Olson complex of *Prosthecochloris aestuarii* determined by temperature-dependent absorption and fluorescence line-narrowing measurements. *J. Phys. Chem. B* **104**, 5825–5831 (2000).
25. Lee, H., Cheng, Y.-C. & Fleming, G. R. Coherence dynamics in photosynthesis: protein protection of excitonic coherence. *Science* **316**, 1462–1465 (2007).
26. Olbrich, C., Strumpfer, J., Schulten, K. & Kleinekathofer, U. Quest for spatially correlated fluctuations in the FMO light-harvesting complex. *J. Phys. Chem. B* **115**, 758–764 (2011).
27. Shim, S., Rebentrost, P., Valleau, S. & Aspuru-Guzik, A. Atomistic study of the long-lived quantum coherences in the Fenna–Matthews–Olson complex. *Biophys. J.* **102**, 649–660 (2012).
28. Maiuri, M., Ostroumov, E. E., Saer, R. G., Blankenship, R. E. & Scholes, G. D. Coherent wavepackets in the Fenna–Matthews–Olson complex are robust to excitonic-structure perturbations caused by mutagenesis. *Nat. Chem.* **10**, 177–183 (2018).

© 2018 Macmillan Publishers Limited, part of Springer Nature. All rights reserved.

29. Rätsep, M. & Freiberg, A. Electronphonon and vibronic couplings in the FMO bacteriochlorophyll a antenna complex studied by difference fluorescence line narrowing. *J. Lumin.* **127**, 251–259 (2007).
30. Rätsep, M., Cai, Z.-l, Reimers, J. R. & Freiberg, A. Demonstration and interpretation of significant asymmetry in the low-resolution and high-resolution *Qy* fluorescence and absorption spectra of bacteriochlorophyll a. *J. Chem. Phys.* **134**, 024506 (2011).
31. Ceccarelli, M., Lutz, M. & Marchi, M. A density functional normal mode calculation of a bacteriochlorophyll a derivative. *J. Am. Chem. Soc.* **122**, 3532–3533 (2000).
32. Christensson, N., Kauffmann, H. F., Pullerits, T. & Mančal, T. Origin of long-lived coherences in light-harvesting complexes. *J. Phys. Chem. B* **116**, 7449–7454 (2012).
33. Tiwari, V., Peters, W. K. & Jonas, D. M. Electronic resonance with anticorrelated pigment vibrations drives photosynthetic energy transfer outside the adiabatic framework. *Proc. Natl. Acad. Sci. USA* **110**, 1203–1208 (2013).
34. Tempelaar, R., Jansen, T. L. C. & Knoester, J. Vibrational beatings conceal evidence of electronic coherence in the FMO light-harvesting complex. *J. Phys. Chem. B* **118**, 12865–12872 (2014).
35. Augulis, R. & Zigmantas, D. Two-dimensional electronic spectroscopy with double modulation lock-in detection: enhancement of sensitivity and noise resistance. *Opt. Express* **19**, 13126–13133 (2011).
36. Fuller, F. D. et al. Vibronic coherence in oxygenic photosynthesis. *Nat. Chem.* **6**, 706–711 (2014).
37. Romero, E. et al. Quantum coherence in photosynthesis for efficient solar-energy conversion. *Nat. Phys.* **10**, 676–682 (2014).
38. Hochstrasser, R. M. Two-dimensional IR-spectroscopy: polarization anisotropy effects. *Chem. Phys.* **266**, 273–284 (2001).
39. Zanni, M. T., Ge, N.-H., Kim, Y. S. & Hochstrasser, R. M. Two-dimensional IR spectroscopy can be designed to eliminate the diagonal peaks and expose only the crosspeaks needed for structure determination. *Proc. Natl. Acad. Sci. USA* **98**, 11265–11270 (2001).
40. Westenhoff, S., Palecek, D., Edlund, P., Smith, P. & Zigmantas, D. Coherent picosecond exciton dynamics in a photosynthetic reaction center. *J. Am. Chem. Soc.* **134**, 16484–16487 (2012).
41. Paleček, D., Edlund, P., Westenhoff, S. & Zigmantas, D. Quantum coherence as a witness of vibronically hot energy transfer in bacterial reaction center. *Sci. Adv.* **3**, e1603141 (2017).
42. Duan, H.-G. et al. Nature does not rely on long-lived electronic quantum coherence for photosynthetic energy transfer. *Proc. Natl. Acad. Sci. USA* **114**, 8493–8498 (2017).
43. Li, H., Bristow, A. D., Siemens, M. E., Moody, G. & Cundiff, S. T. Unraveling quantum pathways using optical 3D Fourier-transform spectroscopy. *Nat. Commun.* **4**, 1390 (2013).
44. Seibt, J., Hansen, T. & Pullerits, T. 3D spectroscopy of vibrational coherences in quantum dots: theory. *J. Phys. Chem. B* **117**, 11124–11133 (2013).
45. Butkus, V. et al. Discrimination of diverse coherences allows identification of electronic transitions of a molecular nanoring. *J. Phys. Chem. Lett.* **8**, 2344–2349 (2017).
46. Thyrhaug, E. et al. Ultrafast coherence transfer in DNA-templated silver nanoclusters. *Nat. Commun.* **8**, 15577 (2017).
47. Fransted, K., Caram, J. R., Hayes, D. & Engel, G. S. Two-dimensional electronic spectroscopy of bacteriochlorophyll a in solution: elucidating the coherence dynamics of the Fenna–Matthews–Olson complex using its chromophore as a control. *J. Chem. Phys.* **137**, 125101 (2012).
48. Mukamel, S *Principles of Nonlinear Optical Spectroscopy* (Oxford Univ. Press, Oxford, 1995).
49. Butkus, V., Zigmantas, D., Valkunas, L. & Abramavicius, D. Vibrational vs. electronic coherences in 2D spectrum of molecular systems. *Chem. Phys. Lett.* **545**, 40–43 (2012).
50. Orlandi, G. & Siebrand, W. Theory of vibronic intensity borrowing. Comparison of Herzberg–Teller and Born–Oppenheimer coupling. *J. Chem. Phys.* **58**, 4513–4523 (1973).
51. Dostál, J., Mančal, T., Vácha, F., Pšenčík, J. & Zigmantas, D. Unraveling the nature of coherent beatings in chlorosomes. *J. Chem. Phys.* **140**, 115103 (2014).
52. Kano, H., Saito, T. & Kobayashi, T. Observation of Herzberg–Teller-type wave packet motion in porphyrin J-aggregates studied by sub-5-fs spectroscopy. *J. Phys. Chem. A* **106**, 3445–3453 (2002).
53. Dostál, J., Mančal, T., Vácha, F., Pšenčík, J. & Zigmantas, D. Unraveling the nature of coherent beatings in chlorosomes. *J. Chem. Phys.* **140**, 115103 (2014).
54. Wen, J., Zhang, H., Gross, M. L. & Blankenship, R. E. Membrane orientation of the FMO antenna protein from *Chlorobaculum tepidum* as determined by mass spectrometry-based footprinting. *Proc. Natl Acad. Sci. USA* **106**, 6134–6139 (2009).
55. Wahlund, T. M., Woese, C. R., Castenholz, R. W. & Madigan, M. T. A thermophilic green sulfur bacterium from New Zealand hot springs, *Chlorobium tepidum* sp. nov. *Arch. Microbiol.* **156**, 81–90 (1991).
56. Holstein, T. Studies of polaron motion. *Ann. Phys.* **8**, 325–342 (1959).
57. Olbrich, C. et al. From atomistic modeling to excitation transfer and two-dimensional spectra of the FMO light-harvesting complex. *J. Phys. Chem. B* **115**, 8609–8621 (2011).
58. Jansen, T. L. C. & Knoester, J. Nonadiabatic effects in the two-dimensional infrared spectra of peptides: application to alanine dipeptide. *J. Phys. Chem. B* **110**, 22910–22916 (2006).
59. Torii, H. Effects of intermolecular vibrational coupling and liquid dynamics on the polarized Raman and two-dimensional infrared spectral profiles of liquid *N*,*N*-dimethylformamide analyzed with a time-domain computational method. *J. Phys. Chem. A* **110**, 4822–4832 (2006).

Acknowledgements

The work in Lund was supported by the Swedish Research Council, the Knut and Alice Wallenberg Foundation and the Crafoord Foundation. R.T. acknowledges The Netherlands Organisation for Scientific Research (NWO) for support through a Rubicon grant. D.B. acknowledges funding from Czech Science Foundation under grant no. P501/12/G055 and institutional support RVO:60077344. We thank D. Paleček for making available his code for complex QB analysis.

Author contributions

D.Z. conceived the idea, E.T., M.J.P.A., K.Z. and D.Z. designed and performed experiments, R.T., J.K. and T.L.C.J. designed the theory, R.T. performed simulations and D.B. extracted and purified the sample. E.T., M.J.P.A. and R.T. analysed the data. E.T., R.T. and D.Z. wrote the manuscript with input from all the other authors.

Competing interests

The authors declare no competing financial interests.

Additional information

Supplementary information is available for this paper at https://doi.org/10.1038/s41557-018-0060-5.

Reprints and permissions information is available at www.nature.com/reprints.

Correspondence and requests for materials should be addressed to D.Z.

Publisher's note: Springer Nature remains neutral with regard to jurisdictional claims in published maps and institutional affiliations.

© 2018 Macmillan Publishers Limited, part of Springer Nature. All rights reserved.